17th World Conference on Earthquake Engineering, 17WCEE

Sendai, Japan - September 13th to 18th 2020

MODEL CONSTRUCTION OF JAPANESE TRADITIONAL WOODEN HOUSES FOR DAMAGE PREDICTION BASED ON MEASURED NATURAL FREQUENCIES AND FIELD EXPERIMENT

T. Yagi[1], E. Ito[2], and H. Kawase[3]

[1] *Employee, Electric Power Development Co.,Ltd., takachika_yagi@jpower.co.jp*
[2] *Program-Specific Researcher, DPRI Kyoto university, ito@sere.dpri.kyoto-u.ac.jp*
[3] *Program-Specific Professor, DPRI Kyoto university, kawase@sere.dpri.kyoto-u.ac.jp*

Abstract

After the 1995 Hyogo-ken Nanbu (Kobe) earthquake crustal earthquakes have been occurring frequently in Japan and people in the near field have been suffered severe damages. It is very important to study earthquake disaster prevention countermeasures in Japan, including strong motion prediction and structural damage prediction. In order to predict strong ground motions with high accuracy, seismic waveforms recorded by an advanced seismic observation network in the near field are necessary. However, such accumulated waveforms are about 30, which are still not sufficient to estimate the level of strong ground motions with high accuracy. Recently, researchers try to reproduce waveforms of historical earthquakes which were not measured, based on the old documents in order to increase numbers of strong ground motions in the near field.

The purpose of this paper is to construct a dynamic response analysis model of Japanese traditional wooden houses, especially built before 1900, for a historical earthquake damage estimation in order to reproduce destruction processes near the epicenters for more quantitative evaluation of strong ground motions. We constructed this model based on the natural frequency characteristics of wooden houses and a pull-down field experiment of a more than 130-year-old house.

From a pull-down (static) experiment of a more than 130 years-old traditional wooden house, we found that the maximum shear strength of the house was 102 kN at the story drift angle of 0.0078 rad. We also found that the house could sustain the maximum relative displacement of 300 mm (0.037 rad. in terms of the story drift angle) which was the pull-down limit from the separation distance to the resisting frame. The shear strength at this maximum deformation level remained to be 78 kN. By using a 3-D full-frame static analysis code we can successfully reproduce nonlinear behavior of the house until the sudden loss of strength in one member.

Keywords: Wooden Structure, Damage Prediction, Pull-Down Experiment, Historical Earthquake

1. Introduction

Japan is one of the most earthquake-prone countries in the world. Earthquake activity in the southwestern Japan has been especially vigorous after the 1995 Hyogo-ken Nanbu (Kobe) Earthquake. Many large inland earthquakes causing severe damage have happened since then, including the 2000 Tottori Earthquake, the 2005 West Off Fukuoka Prefecture Earthquake, and the 2016 Kumamoto Earthquake. Therefore, earthquake damage prevention and mitigation research is very important to us living in Japan.

An important pillar of earthquake damage prevention and mitigation research is strong motion prediction that predicts vibration of the ground generated at a presumed fault plane. Microscopic fault parameters are important to conduct this strong motion prediction with high accuracy, and the parameters can be obtained using waveform inversion of records from modern earthquake observation networks. The Japan Meteorological Agency, the National Research Institute for Earth Science and Disaster Resilience (NIED), and local governments established modern strong motion observation networks in Japan after the 1995 Hyogo-ken Nanbu (Kobe) Earthquake and have been continuously observing earthquakes since then. However, the number of records from the seismic observation networks of strong motions from inland earthquakes that caused damage is about 30 cases at most. The number of earthquake records over magnitude 7.0, which cause especially large damage, is far from sufficient. Therefore, a couple of attempts to reproduce the seismic source process of historical earthquakes in the literature are recently reported. Unveiling the seismic source process of historical earthquakes based on existing literature would improve strong motion prediction accuracy and ultimately enhance the quality of damage prevention and mitigation measures in Japan.

For example, Kanda et al. (2003) [1] obtained the sources of short period energy release in the past Nankai Trough mega-quakes using seismic intensity as the target. They found before the 2011 off the Pacific Coast of Tohoku Earthquake that short period components are not uniformly released from the fault plane. The target of their inversion is the intensity values at several sites determined from the damage in the past mega-quakes. The method to estimate the intensity was the attenuation relationships of the JMA seismic intensity derived from the contemporary strong motion data. Their equivalence has never been proved, Manpo et al. (2018) [2] recently applied strong motion simulations over a wide frequency range using a hybrid method on the 1662 Ohmi-Wakasa Earthquake. They pointed out that the magnitude of this earthquake could be large (M7.45) among the conventional range of estimation. However, the estimated magnitude from damage in the literature and the estimated measured intensity from the strong motion waveform were considered equivalent in their study, thus most of the precious information in the waveform has not been used. Therefore, re-evaluation of the seismic source process of past historical earthquakes mostly uses current intensity measurements and recorded structural damages have not been directly targeted.

Our ultimate goal to address this issue is to re-evaluate the strong motion generation process of historical earthquakes, in particular, the seismic source process of inland earthquakes where the strong motion near the focus played a crucial role. We first investigated the static nonlinear behavior of a traditional wooden house and then established a seismic damage estimation model where seismic motion was given as an input. Static loading experiments were conducted on a traditional wooden house in Okayama Prefecture (denoted as IBR01 in this paper). The obtained yielding shear force and deformation performance as well as results of simulations using a three-dimensional frame model are reported.

2. Basic vibration characteristics of the traditional wooden house

A field survey was conducted that included continuous microtremor measurements. Mass appraisal of IBR01 was also conducted and its details are described in the next section.

Microtremor measurement were conducted using equipment combining SMAR-6A3P (former Akashi, currently Mitutoyo Corporation), which is a portable three-axis acceleration seismometer containing an amplifier with amplification ratio of 0.1 to 10,000 times, and data recording device LS-8800 (Hakusan Corporation). Accelerometers were installed at the entrance on the first story and on a horizontal beam behind the ceiling of the house. The measured Fourier spectral ratio of the second story or the beam to the first story was used to obtain the resonance frequency of the first story of the traditional wooden houses. The sampling frequency was 100 or 200 Hz, the amplification was usually set to be 500 times, and the observation duration was at least 15 minutes.

Figure 1 shows the first story plan of IBR01 and Fig. 2 gives photos of the house. IBR01 was built around 1888. The last resident left about 20 years ago, and the house was empty at the time of the experiment. This building had a hip-and-gable roof with four main rooms. Laths were laid out on the attic, which were covered with hardened soil with a thickness about 5 cm. The roof was thatched but covered with a corrugated tin plate for protection. Pantiles were used in the roof at X1-X2, X9-X10, and Y1-Y2 planes, and these parts were probably remodeled and/or added after initial construction. In particular, part of the wall of the X9 and X10 planes was not a mud wall. Instead, there were walls where concrete blocks were stacked and cement was poured in the gaps, and where wooden boards were pasted on the mud wall and the surface was reinforced by coating with mortar.

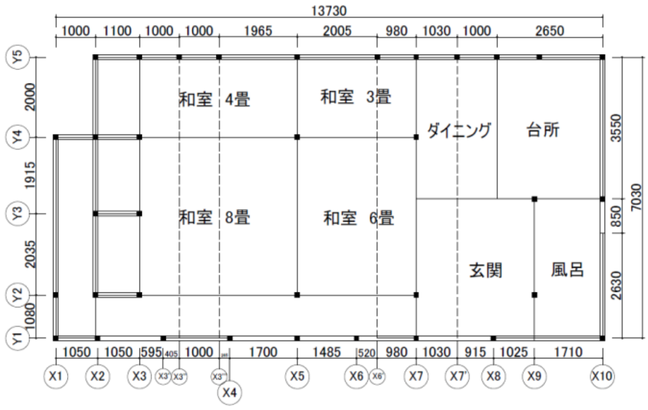

Fig. 1 – Plan of the traditional wooden house used for the pull-down experiment, IBR01.

Fig. 2 – Photos of inside and outside of IBR01 used for the pull-down experiment.

Table 1 shows the fundamental resonant frequencies obtained from microtremor measurement of IBR01. Measurements of IBR01 were taken before (No. 1) and after (No. 2) the static loading experiments. Microtremor measurement equipment was installed on the earth floor of the first story and on a horizontal member in the attic at point X9Y3 on the plan, and additionally also on the soil in the attic at point X3Y3 for the measurement after the experiments. The results from the two attic measurements did not differ much, thus the results for the common measurement point X9Y3 are shown in Table 1. The resonance frequency before the experiments was large compared to other traditional wooden houses, which is usually in between

2 to 2.5 Hz. This is probably because of the effect from the concrete block wall in the added portion that is discussed later.

Table 1 – Observed predominant frequency of IBR01(Hz).

No.	State	Short span	Long span
1	Before exp.	3.98	5.03
2	After exp.	2.69	3.63

3. Mass assessment of traditional wooden house IBR01

The building mass was assessed before the static loading experiments to make calculation of the base shear coefficient possible. The dimensions of the members in IBR01 were measured using tape measures and a laser range finder. The building area was 94.52m^2 in footprint. Columns and beam members in a traditional wooden house are irregular-shaped. Therefore, the dimensions were measured at three locations, which are both ends and the center, and the average was used as the dimensions of the member for calculations. The member volume from measurement results and the mass per unit volume were multiplied to assess the building mass. All timber was assumed to be Japanese cedar, which has a density of 0.38g/cm^3 according to the reference [3]. The density of the mud wall was set to 1.4 g/cm^3 based on the reference [4]. The roof load per floor area for thatched and pantile roofs were set to 1500 and 2400 N/m^2, respectively, as in the reference [5]. Table 2 shows the results of member dimension measurement and the mass assessment. The mass of IBR01 was assessed as 31.58 t. Pine, Japanese cypress, and cypress could have been used as main members instead of Japanese cedar. However, their density are in the range of 0.41-0.53 g/cm^3, and the composition of timber is small at about 6%. Therefore, the effect of choice of the timber species on the total mass is estimated to be 1% at most.

Table 2 – Estimated mass of IBR01.

Member		Mass (kg)		
Structure	Column	384	Sub Total 14,925	Total 31,577
	Beam	1,766		
	Wall	12,776		
Roof		16,652		

4. Static loading experiments

Static loading experiments were conducted as follows. There is a cliff in front of and at the back of IBR01, thus loading was possible only from one direction from the front side because of this geographical restriction. A C-channel steel beam was placed in contact with a wooden beam at height 2,271 mm from the ground at the Y5 plane of IBR01. A reaction structure set up in front of the house was connected by wires to four points on the steel frame as illustrated in Fig. 3. Chain blocks and load cells were placed between the wires and the reaction structure, and loading was conducted by controlling the chain blocks. Fig. 4 shows the arrangement of measuring equipment.

Static loading experiments were conducted over two days. Experiment (1) in the elastic regime was performed on the first day, and a large deformation experiment (2) with loading up to a maximum interstory displacement of 300 mm was conducted on the second day. The loading schedule, maximum horizontal force, and maximum displacement between stories for experiments (1) and (2) are shown in Table 3.

The loading schedules are described below. Eight loading schedules, which are 1-1 to 1-8, were employed in experiment (1). The two load cells to the left and right (see Fig. 7 for the load cells labeled LC_RT and LC_LF) were uniformly loaded in schedules 1-1 to 1-6. There was almost no deformation in the X10 plane because of the retrofitted concrete block wall, thus only LC_RT, which is on the X10 plane side, was loaded in schedule 1-7. The deformation of the X10 plane was still very small, thus cracks were made with a hammer in the concrete block wall of the X10 plane prior to loading schedule 1-8. As a result, the displacement of the X10 plane increased to about half of the X2 plane.

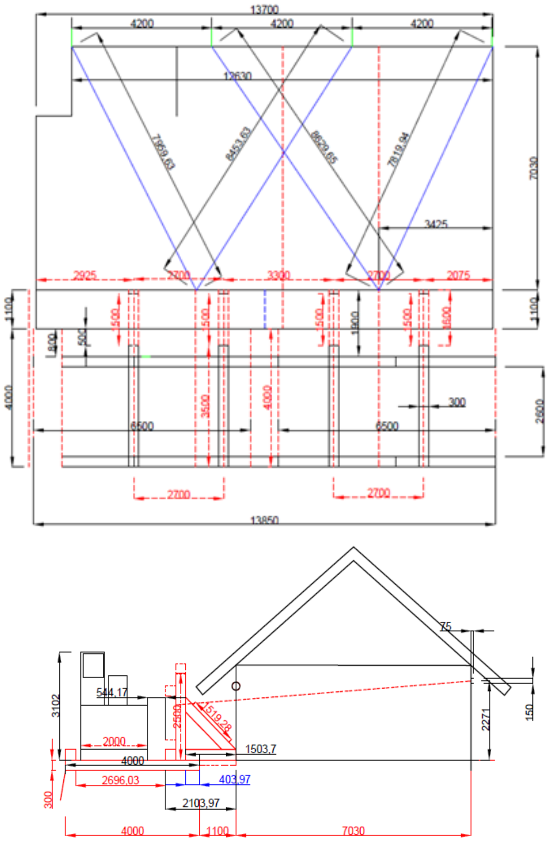

Fig.3 – Pull-down test plan and elevation.

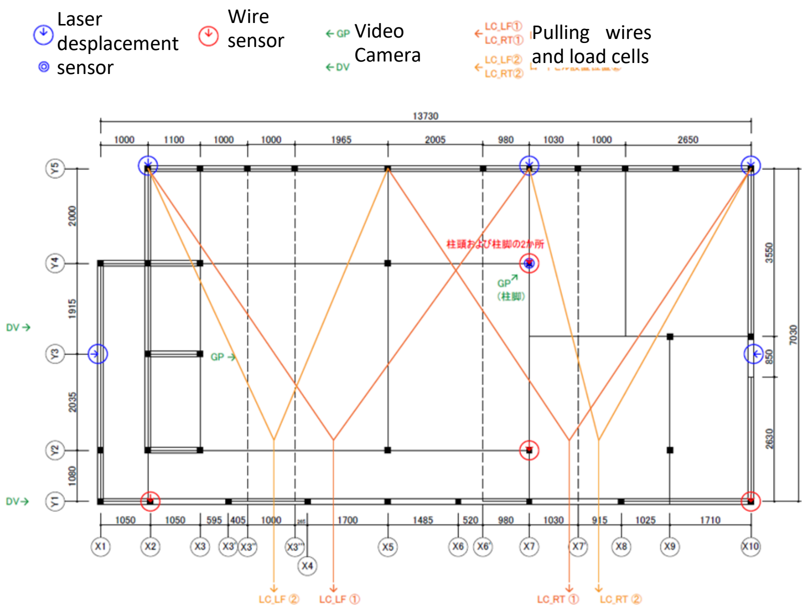

Fig. 4 – Pulling wires, displacement sensors, and cameras.

Table 3 – Experiment schedule and measured results.

Experiment (1)						
No.	Name	Time	Target	Observed (kN)	Story drift (rad.)	
					X2Y1	X10Y1
1-1	8kN	13:00-13:15	8kN	8.0	0.0005	0.0002
1-2	16kN	13:28-13:35	16kN	17.2	0.0011	0.0004
1-3	24kN	13:35-13:40	24kN	26.0	0.0022	0.0004
1-4	32kN_1	13:40-13:50	32kN	32.4	0.0036	0.0005
1-5	48kN	13:50-13:55	48kN	49.0	0.0084	0.0011
1-6	64kN_1	13:55-14:00	64kN	65.0	0.0176	0.0016
1-7	90kN_1	14:00-14:15	90kN	93.6	0.0233	0.0061
1-8	90kN_2	14:15-14:30	90kN	78.4	0.0228	0.0108

Experiment (2)						
No.	Name	Time	Target	Observed (kN)	Story drift (rad.)	
					X2Y1	X10Y1
2-1	32kN_2	8:40-8:44	32kN	32.6	0.0065	0.0016
2-2	64kN_2	8:47-8:50	64kN	63.8	0.0138	0.0029
2-3	96kN	8:55-9:00	96kN	98.2	0.0380	0.0050
2-4	112kN	9:00-9:30	112kN	94.8	0.0535	0.0066
2-5	100kN_1	9:30-9:50	100kN	100.6	0.0692	0.0088
2-6	100kN_2	9:55-10:10	100kN	102.2	0.0820	0.0276
2-7	100kN_3	10:10-11:00	100kN	93.4	0.0902	0.0416
2-8	100kN_4	11:00-12:00	200 ㎜	83.2	0.0924	0.0909
2-9	100kN_5	12:00-12:30	300 ㎜	87.4	0.1360	0.1266

Nine loading and unloading schedules, which are 2-1 to 2-9, were employed in experiment (2). The two load cells were uniformly loaded in schedules 2-1 to 2-5. In schedule 2-5, the X2 plane continued to significantly deform compared to the X10 plane even though the maximum horizontal force reached 100 kN. Therefore, the position of wires at IBR01 was changed from LC_RT(1) and LC_LF(1) to LC_RT(2) and LC_LF(2) as shown in Fig. 4. Schedule 2-6 was loaded after this change. However, the deformation of the X2 plane was still large after loading 20 kN on LC_LF in schedule 2-6. Therefore, only LC_RF was loaded further while the load was kept the same in LC_LF. The maximum yield force was attained in this schedule 2-6. The subsequent loading schedules loaded 20 kN to LC_LF and LC_RT and then additionally loaded LC_RT only. The X2 frame significantly deformed compared to the X10 frame again in schedule 2-7. Therefore, the mortar wall pasted on the mud wall in the X9 frame was removed before loading schedule 2-8. Furthermore, most of the concrete block wall in the X10 frame was removed before loading schedule 2-9. As

Fig.5 – An example of inclined situation during 2-5 experiment.

a result, the resisting force saturated when LC_RT and LC_LF reached 50 and 25 kN, respectively. Subsequently, only deformation increased, and ultimately the maximum displacement reached 300 mm. The experiment was stopped at this point. Fig. 5 shows the deformation during loading schedule 2-5.

Figs. 6 and 7 show measured horizontal load results of the two load cells during a representative loading schedule in experiment (1) and (2), respectively. The horizontal axis is the time after initiating loading. LC_LF and LC_RT are the measured values in the two load cells, and LC_SM is their sum. Figs. 8 and 9 show the in-plane horizontal displacement at a representative measurement point in experiments (1) and (2), respectively. The vertical axis is the total horizontal load LC_SM. The wire displacement gauge for X2Y1 was installed in the loading direction, thus the values are negative.

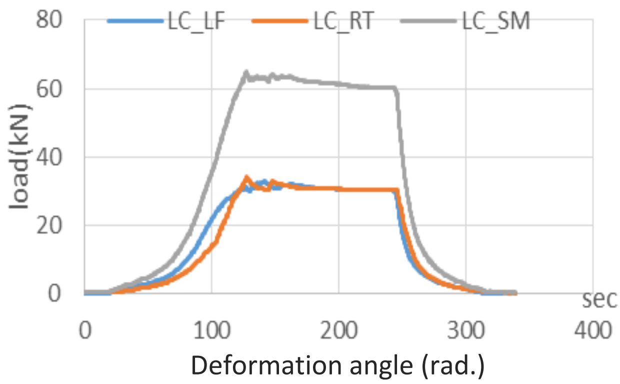

Fig.6 – Loading time history for 1-6 experiment.

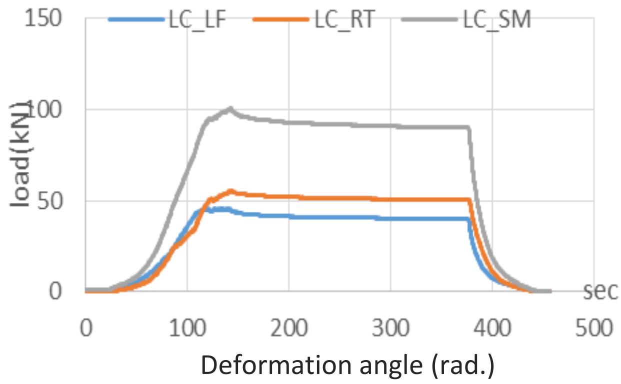

Fig.7 – Loading time history for 2-5 experiment.

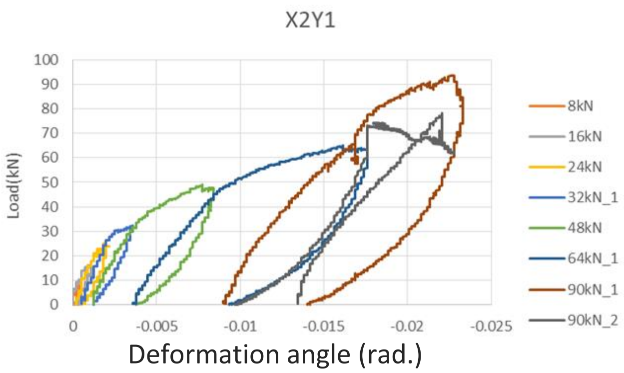

Fig.8 – An example of applied horizontal force and observed deformation angle for series No.1.

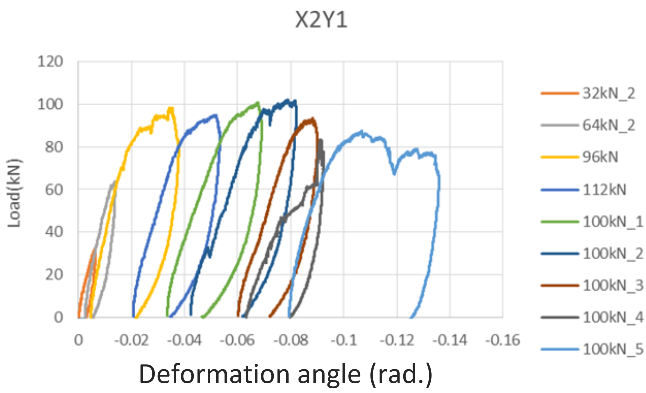

Fig.9 – An example of applied horizontal force and observed deformation angle for series No.2.

Pillar bottom displacements and out-of-plane displacements were also measured. There was almost no displacement at the pillar bottoms. The out-of-plane displacements increased with increasing in-plane displacement, but the former was less than 1/5 of the latter. The building apparently underwent shear deformation and very small torsion. The angle of torsion in loading schedule 2-5 was about 0.01 rad.

The results of static loading experiments on IBR01 can be summerized as follows. The maximum proof strength was 102kN and the average in-plane interstory horizontal deformation angle was 0.055 rad. The maximum yield force was 0.32 when converted to the base shear coefficient. The horizontal yield force at interstory displacement 300 mm (deformation angle of 0.13 rad.) was 78 kN, which corresponds to the base shear coefficient of 0.25. Thus, the target traditional wooden house has good deformation properties because it sustained heavy weight under a horizontal deformation angle larger than 0.1 rad.

5. Simulation analysis

Analysis to reproduce the static loading experiments were conducted by incremental analysis using SNAP, an elasto-plastic analysis code for a three-dimensional frame with an arbitrary form. SNAP can perform dynamic response analysis, stress analysis, and incremental elasto-plastic analysis at the member level in structures with an arbitrary form. SNAP has been used in reproduction analysis of static loading experiments in a new full-scale wooden test building, and its validity has been demonstrated [6]. This reproduction analysis built a model that can trace the displacements at X2Y1 and X10Y1 during experiments.

The static loading experiments installed wires to the traditional wooden house IBR01 at a height of 2,271 mm and loaded at this position. Therefore, the model was built up to a height of 2,271 mm. No model was considered above this height. Instead, a rigid floor was assumed at this height. The differences between the average displacement of the planes, which presumes a rigid floor, and the measured displacement of each plane was less than 20%. The X1 plane was added later after the initial construction, and there was severe damage, thus this plane was not included in the model, which means that we modeled the main part from X2 to X10 planes. Pin joints were used for all joints. Fig. 10 shows the model for our analysis, while Fig. 11 gives a layout drawing of walls. The green parts are mud walls, the yellow parts are mud walls where wooden boards are pasted on mud walls and then reinforced by coating with mortar (hereafter ”reinforced clay wall”), and the orange parts are concrete block (CB) walls.

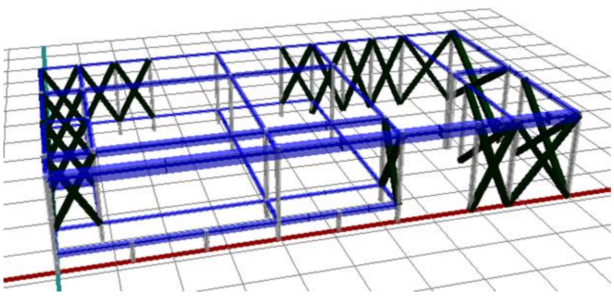

Fig.10 – A 3-D full-frame model used for simulation.

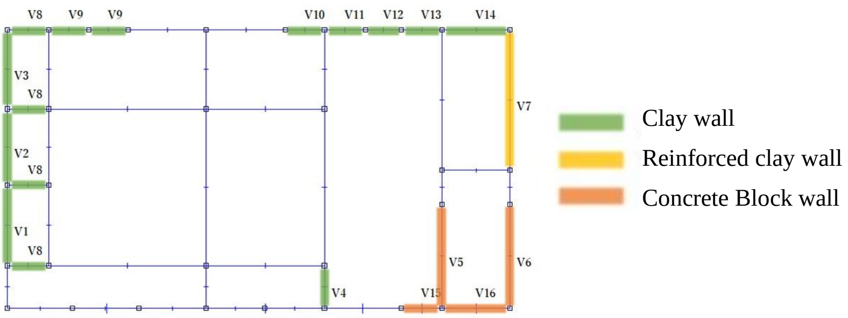

Fig. 11 – Locations of walls assumed in the simulation.

Clay walls were modeled by brace substitution. The parameters of the substituting braces were set by calculating the cross-section of braces such that the initial stiffness of the Clay wall over one span was preserved.

The skeleton curve of the clay wall was modeled using four connected lines as shown in Fig. 12. This is based on the clay-plastered wall model by Maekawa et al. [7]. Here, σ_{tw} is the shear strength, which is 0.0785 N/mm^3 in the clay-plastered wall model in Maekawa et al. [7]. Needless to say, this parameter depends on the member. The shear strength of the clay wall in this study was set to 0.0432 N/mm^3 to reproduce the experimental results. This is 55% of the shear strength of the clay-plastered wall model in Maekawa et al. Hysteresis characteristics were based on the normally consolidation line (NCL) model for wooden buildings consisting of four connected lines [8]. The characteristic loop of this NCL model for wooden buildings was expressed as a high order polynomial curve in Eq. (1) below. Here, the maximum experienced displacement is scaled to unity. The various coefficients in the equation were identified such that the experimental results can be reproduced. The specifications of the obtained clay wall model are shown in Table 5.

$$L(x) = (B|x|^n + 1 - B)x \mp A(x^4 - 1) \quad (-1 \leq x \leq 1) \tag{1}$$

Here, A is the load at the intercept (0 ≤A≤1), 1-B is the gradient at the intercept (0≤B≤1), n is a natural number that is 2 or larger, and x is the relative displacement.

Table 4 – Model parameter for the clay walls.

Thickness	60 mm
Young's modulus E	65 N/mm^2
Shear stength σ_{tw}	0.0785 N/mm^3×0.55
Force at zero displacement A	0.35
B in Eq. (1)	0.4
n for loading process	2
n for unloading process	10

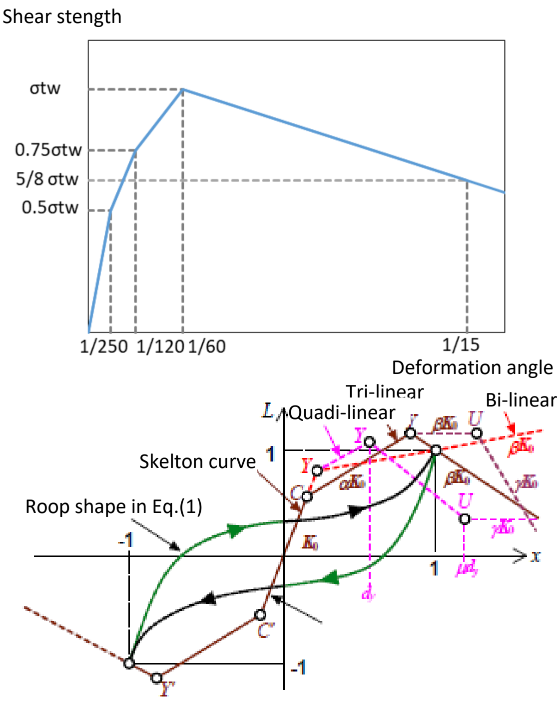

Fig.12 – Model properties of the clay walls [7].

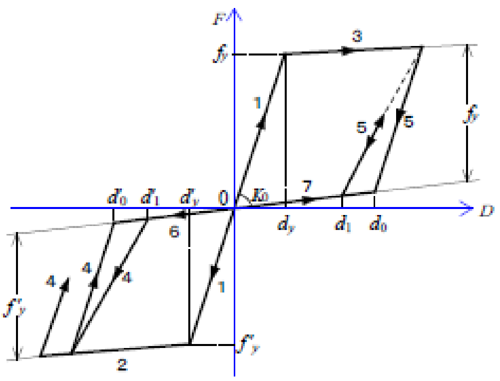

Fig.13 – Nonlinear characteristics of the CB wall.

The reinforced clay wall and CB wall were substituted with braces similar to those for the clay wall. The hysteresis characteristics for the reinforced clay wall were the NCL model for wooden buildings consisting of four connected lines, and those of the CB wall were a bi-linear slip-type model. Fig. 13 shows the restoring force characteristics of the CB wall. Assuming the yield level at interstory deformation angle 1/120 rad., the stiffness reduction rate β was set to be 0.6 from trial and error to reproduce the experimental results. The cross-section area was assumed to be the same as the clay wall, and the Young's modulus E was increased such that the results of analysis in the elastic regime matched those from the experiments. The Young's modulus of the reinforced clay walls was set to that of the CB wall, which is necessary to set 445 N/mm^2 to reproduce the experimental results.

Analysis to reproduce the static loading experiments was conducted using the models designed above. Loading schedules 2-1 to 2-3 in experiment (2) were analyzed. The deformation of left and right sides were made uniform to some extent in the last schedule of experiment (1), which is 1-8, therefore, we believe that the subsequent experimental results should reflect the intrinsic deformation characteristics of the house. There remains the final residual deformation of 0.009 rad in experiment (1), thus the elasticity limit was slightly exceeded. However, the hysteresis in experiments (1) and (2) with small deformation were almost the same, inferring that there was no significant damage up to schedule 2-3, where some members may have received damage as shown later.

Fig. 14 shows the input load time history curve from the experimental results. The input load to the computational model was the measured input in load cells that was equally distributed to the two points where wires were secured. During loading of schedule 2-3, the load decreased and the deformation increased after a large breaking sound (time Ty in the figure). Some members of the building could have been damaged, and the building became significantly nonlinear beyond the point, thus the time history from schedules 2-1 to 2-3 were reproduced until that time.

The reproduction analysis results are shown in Figs. 15 and 16. EXP and SNAP in the figures represent experimental and analyzed results, respectively. The skeleton curves in the experimental results are reproduced well in the analysis. However, the X2 plane slightly overestimated the maximum displacement under loading schedule 2-2 compared to experimental results. In contrast, the experimental values were almost completely reproduced in the X10 plane. The analyzed unloading loop in schedule 2-3, which is after the building yielded and the maximum input load in the experiments was attained, differed from experimental results in both X2 and X10 planes. The reason was because the horizontal force loaded on the members was released due to damage to the members. Thus, deformation progressed, and the horizontal resistant force decreased quickly. Quasi-static tracking of sudden generation of unbalanced forces from damage to members is difficult, and the deformation after damage to some members could not be followed.

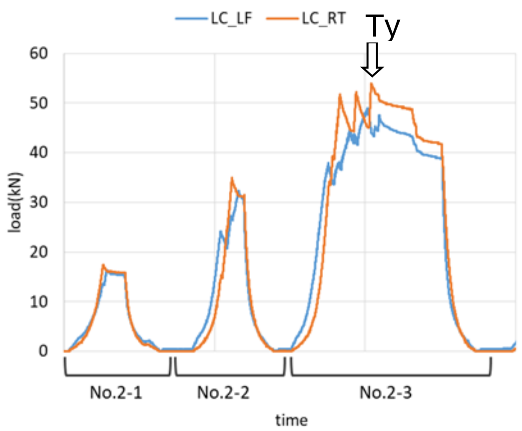

Fig.14 – Input horizontal force time history for experiments 2-1, 2-2, and 2-3 used for simulation. Ty is the time when a part of the member was broken.

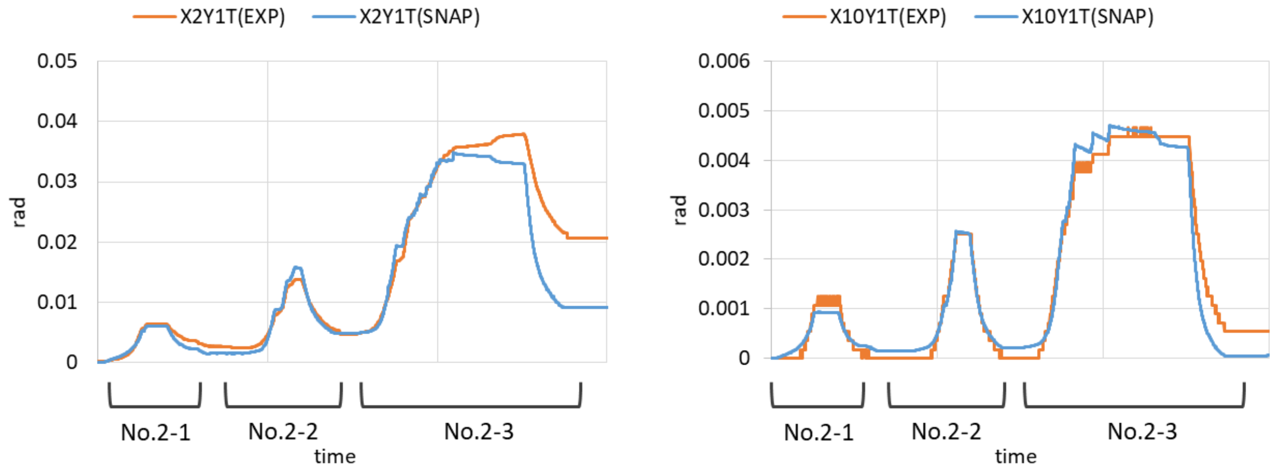

Fig.15 – Observed and simulated story drift time histories at two sections on the left and right.

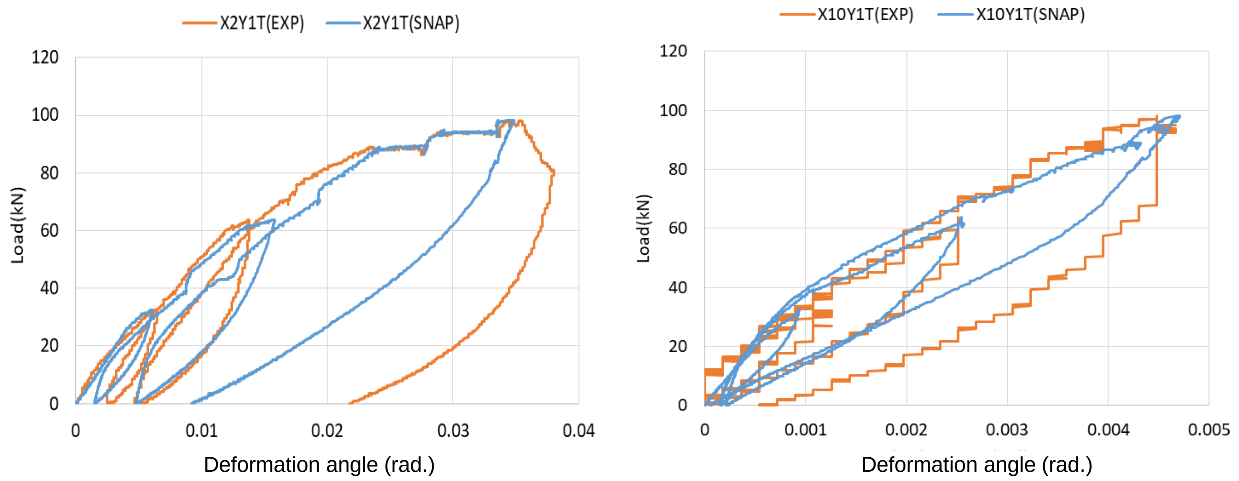

Fig.16 – Observed and simulated nonlinear behaviors at two sections on the left and right.

We estimated that damage of some members happened immediately before unloading in schedule 2-3, which is evident because the residual deformation after unloading was significantly larger than after previous unloadings. The maximum deformation angle was about 1/30, which corresponds to the level of a total collapse according to the past research [9]. Therefore, the analytic model established in this study reproduces behavior of a traditional wooden house under nonlinear horizontal load up to total collapse.

6. Summary and Conclusions

This study summarized the vibration characteristics of the target traditional wooden house IBR01 of about 130 years old in Ihara City, Okayama Prefecture. Results of static loading experiments and reproduction of the results using a three-dimensional frame analysis software were also reported. The following summarizes the results from the above investigation.

1) Static loading experiments on IBR01 showed that the maximum horizontal force was 102kN (equivalent to a base shear coefficient of 0.32), and the inter-story horizontal deformation angle was 0.055 rad. The horizontal force when the inter-story horizontal displacement was 300 mm (deformation angle of 0.13 rad) in the final loading experiment was 78kN (the equivalent base shear coefficient is 0.25).

2) For reproducing the experimental results, wall members were substituted with braces using an NCL model for wooden buildings consisting of four connected lines, and the shear strength was adjusted in a three-dimensional frame analysis code. The behavior in experimental results were well reproduced until some members were damaged (up to an inter-story deformation angle of 1/30). However, the unloading loop after members were damaged could not be reproduced because the horizontal force rapidly decreased and the deformation increased.

We will combine this study and past work that investigated the resonance frequency of traditional wooden buildings. A damage prediction model for traditional wooden houses based on nonlinear response analysis [9] will be established. The validity of the damage prediction model will be confirmed using results of static horizontal loading experiments in this study and then it will be used to understand the source properties of historical earthquakes as mentioned in the introduction.

7. Acknowledgment

The experiments of this study were successfully performed with the significant commitment by T. Yamazaki, S. Kawasaki, T. Okada, and Nomura Juki Co. Ltd. Thanks are extended for students of Nishino Laboratory in the School of Engineering, Kyoto University. A part of the study was supported by the JSPS Grant-in-Aid for Basic Research (B) No.19H02405 and the Core-to-Core collaborative research program of ERI, the Earthquake Research Institute, The University of Tokyo and DPRI, Kyoto University, No.2018-K-02.

References

[1] Katsuhisa Kanda, Takemura Masayuki, Usami Tatsuo (2003): Inversion Analysis of Distribution of Energy Radiated from an Earthquake Fault Based on the Seismic Intensity Data, Zisin (Journal of the Seismological Society of Japan) 2nd ser. 2, 56, 39-58, 2003.2 (in Japanese with English abstract).

[2] Atsundo Manpo, Eri Ito, Hiroshi Kawase, Fumiaki Nagashima (2018): Estimation of seismic source properties based on strong motion simulation of historical earthquakes, 15th Japan Earthquake Engineering Symposium, 2018.12 (in Japanese with English abstract).

[3] Wood Technological Association of Japan (1975): 300 useful timber in the world, edited by the Government Forest Experiment Station Wood Technology Division, Wood Technological Association of Japan, 1975 (in Japanese).

[4] Koji Yamada, Hiroyuki Nakaji, and Yoshiyuki Suzuki (2011): Resistant force characteristic estimation of wooden frames with clay-plastered walls using mud plasters of different strength, J. Struct. Constr. Eng., AIJ, Vol. 76, No. 660, 347-352, 2011.2 (in Japanese with English abstract).

[5] Agency for Cultural Affairs (2012): Implementation Guidance for Basic Seismic Assessment of Important Cultural Properties (Buildings). 2012.6 (in Japanese).

[6] Rie Yamamoto, Hiroshi Kawase, Shinichi Matsushima, Hidetaka Miyake (2014): Experimental and Numerical Studies on One Room Reinforcement Method with Special Attention to Deformability, Summaries of technical papers of Annual Meeting (Kinki), Architectural Institute of Japan, 2014.9 (in Japanese).

[7] Hideyuki Maekawa, Akito Uchida, Naohiyo Kawai (1999): Dynamic Characteristic of Traditional Wooden Building: Part 8: Estimation of Load-displacement Relationships and Natural Frequencies, Summaries of technical papers of Annual Meeting (Chugoku), Architectural Institute of Japan,1999.9 (in Japanese).

[8] Hiroki Matsunaga, Satsuya Soda, Yuji Miyazu (2007): Modeling of restoring force properties of wooden structures and application to dynamic analysis, Proceeding of the architectural research meetings, Kanto Chapter, Architectural Institute of Japan, pp.201-204, 2007.3 (in Japanese).

[9] Kenji Yoshida, Yoshiaki Hisada, Hiroshi Kawase (2004): Construction of dynamic models of Japanese wooden houses for evaluating earthquake damage by considering building age, Summaries of technical papers of Annual Meeting (Hokkaido), Architectural Institute of Japan, Structures II, B-2, 1059-1060, 2004.8 (in Japanese).

